Insignificant buffering capacity of Antarctic shelf carbonates

J. Hauck,[1] K. R. Arrigo,[2] M. Hoppema,[1] G. L. van Dijken,[2] C. Völker,[1] and D. A. Wolf-Gladrow[1]

Received 19 September 2011; revised 19 September 2012; accepted 26 October 2012; published 24 January 2013.

[1] We combined data sets of measured sedimentary calcium carbonate ($CaCO_3$) and satellite-derived pelagic primary production to parameterize the relation between $CaCO_3$ content on the Antarctic shelves and primary production in the overlying water column. $CaCO_3$ content predicted in this way was in good agreement with the measured data. The parameterization was then used to chart $CaCO_3$ content on the Antarctic shelves all around the Antarctic, using the satellite-derived primary production. The total inventory of $CaCO_3$ in the bioturbated layer of Antarctic shelf sediments was estimated to be 0.5 Pg C. This quantity is comparable to the total CO_2 uptake by the Southern Ocean in only one to a few years (dependent on the uptake estimate and area considered), indicating that the dissolution of these carbonates will neither delay ocean acidification in this area nor augment the Southern Ocean CO_2 uptake capacity.

Citation: Hauck, J., K. R. Arrigo, M. Hoppema, G. L. van Dijken , C. Völker, and D. A. Wolf-Gladrow (2013), Insignificant buffering capacity of Antarctic shelf carbonates, *Global Biogeochem. Cycles*, *27*, 11–20, doi:10.1029/2011GB004211.

1. Introduction

[2] The atmospheric CO_2 content has been increasing since the beginning of the Industrial Revolution. In the decade between 2000 and 2009, the atmospheric CO_2 increase averaged 1.9 ppm yr^{-1} due to anthropogenic perturbations of the carbon cycle [*Friedlingstein et al*., 2010; *Global Carbon Project*, 2010]. In that decade, on average, 8.8 ± 1.2 Pg C yr^{-1} was emitted by burning of fossil fuels, cement production, and land-use change. The carbon inventory in the atmosphere, however, increased by only 4.1 ± 0.1 Pg C yr^{-1}. The remaining 4.7 Pg C yr^{-1} was taken up by the land and oceans in about equal amounts [*Friedlingstein et al*., 2010; *Global Carbon Project*, 2010]. Hence, the terrestrial and marine carbon sinks decelerate atmospheric CO_2 increase, and thus slow down anthropogenic climate change.

[3] The increase of inorganic carbon in the oceans reduces pH (a process recently referred to as ocean acidification) and carbonate saturation states (Ω). Once the seawater is undersaturated with respect to calcium carbonate ($CaCO_3$; $\Omega < 1$), carbonate sediments will start to dissolve, thereby releasing carbonate ions. This does not only counteract acidification, but also enhances the capability of the ocean to act as a CO_2 sink. High latitudes are most sensitive to changes in carbon inventories and might be the first regions to experience undersaturation with respect to $CaCO_3$ [*Orr et al*., 2005; *McNeil and Matear*, 2008; *Yamamoto-Kawai et al*., 2009; *Steinacher et al*., 2009]. Within the polar regions, the shallow shelves undergo the largest changes in pH [*Hauck et al*., 2010; *Arrigo et al*., 2008a]. The saturation horizons in the Southern Ocean not only shift upward from the deep ocean. Changes in the saturation state are largest at the surface and combined with already low surface saturation states, undersaturation might occur at the surface before the entire underlying water column is undersaturated [*Hauck et al*., 2010]. Calcareous sediments on the Antarctic shelves might thus provide an initial buffering of ocean acidification, where we refer to buffering by sedimentary carbonates as a negative feedback to acidification of any magnitude. In our definition, buffering does not necessarily mean that pH is maintained at a constant level, yet, if significant, it would delay or temper acidification as compared to a scenario where no $CaCO_3$ is available for dissolution. Whether there is a significant buffer effect is the subject of this study.

[4] Aragonite is the most soluble form of $CaCO_3$, and thus the first candidate for buffering. A circum-Antarctic data compilation revealed that aragonite is an insignificant constituent of Antarctic shelf sediments [*Hauck et al*., 2012] despite the reports of high pteropod (pelagic mollusks that produce aragonite shells) densities in the water column [*Hunt et al*., 2008; *Accornero et al*., 2003]. Almost all samples considered consisted of low-Mg calcites. As the distribution on a subregional scale was patchy and there were data gaps, especially in the southwest Pacific and Indian ocean (swP/IO) sectors of the Antarctic shelves, it is not possible to simply interpolate the $CaCO_3$ data spatially to obtain a circum-Antarctic estimate. A method to predict $CaCO_3$ content based on environmental conditions in the areas with data gaps is crucial to estimate the total inventory of $CaCO_3$ on Antarctic shelves.

[5] $CaCO_3$ is one of the main sedimentary substances, besides lithogenic material, opal, and organic matter. The actual composition of sediments is the result of a complex

[1]Alfred Wegener Institute for Polar and Marine Research, Bremerhaven, Germany.
[2]Department of Environmental Earth System Science, Stanford University, Stanford, California, USA.

Corresponding author: J. Hauck, Alfred Wegener Institute for Polar and Marine Research, Postfach 12 01 61, 27515 Bremerhaven, Germany. (judith.hauck@awi.de)

0886-6236/13/2011GB004211

interplay of various processes. Three main processes determine whether a substance can be found in the sediments. First, there needs to be a source of the material in the water column, i.e., production of the biogenic materials, or another source for lithogenic material, such as atmospheric dust deposition. Second, dissolution or decomposition processes during the sinking through the water column determine how much of the material rains to the seafloor. Third, early diagenetic processes on the seafloor and in the sediment alter its composition and determine the burial in the sediment [*Martin and Sayles*, 2003].

[6] The dissolution or decomposition of the biogenic materials on their way through the water column can be described as a function of the amount of material at the surface (e.g., [*Martin et al*., 1987; *Yamanaka and Tajika*, 1996]). Hence, production in the euphotic zone controls the source terms at the surface and the loss terms in the water column. It is the balance between production at the surface and decay or dissolution at the seafloor that determines how much of the biogenic substances is found in the sediments. Oxic remineralization of organic matter is omnipresent in marine sediments and releases CO_2 [*Martin and Sayles*, 2003]. This leads to metabolic-CO_2 –driven dissolution of $CaCO_3$, as first mentioned by *Berger* [1970]. The relative amounts of $CaCO_3$ and organic matter are further affected by the amount of lithogenic and siliceous material that rain to the seafloor and by bottom currents and winnowing.

[7] We base our analysis on the assumption that $CaCO_3$ production in the euphotic zone and metabolic dissolution of $CaCO_3$ in the sediments are the main processes determining how much $CaCO_3$ is present in the sediments [*Martin and Sayles*, 2003]; this is, of course, a simplification of processes in the real world. $CaCO_3$ production and metabolic dissolution are by definition related to primary production (PP), as none of them would exist without organic matter production or deposition. We hypothesize that increasing PP leads to more $CaCO_3$ production, at least at low PP levels, as $CaCO_3$ production cannot happen without organic matter production. However, increasing PP also leads to more rain of organic matter to the seafloor, and subsequently to more organic matter oxidation and possibly metabolic $CaCO_3$ dissolution.

[8] We made use of the above-mentioned concepts and tried to derive a parameterization of sedimentary $CaCO_3$ as a function of satellite-based estimates of PP and water depth. Applying the parameterization, we use PP as a proxy to map the abundance of carbonates in Antarctic shelf sediments. Based on these maps, we estimate the contemporary $CaCO_3$ inventory, which would be available for dissolution when a reduced bottom water calcite saturation state due to anthropogenic CO_2 uptake would lead to pore water undersaturation in the regions where $CaCO_3$ is nowadays preserved.

2. Data and Fitting Procedure

[9] A set of 390 measurements of the $CaCO_3$ content of surface sediments in continental shelves all around Antarctica was presented in *Hauck et al*. [2012]. Their compilation included both newly measured and literature data. In this analysis, these data were combined with circum-Antarctic calculations of upper ocean PP data based on satellite observations of surface chlorophyll concentrations, sea surface temperature, and sea-ice cover [*Arrigo et al*., 2008b] to estimate large-scale distributions of sediment $CaCO_3$. PP was calculated daily at 4 km horizontal resolution for all Antarctic waters south of 50°S. Daily values at each grid point were integrated over the year to derive annual estimates of PP. The chlorophyll and PP algorithms were validated against a vast amount of field data, including extensive data sets of shelf and coastal areas. The uncertainty of this method was estimated to be less than 10% with respect to chlorophyll and within 25% for PP [*Arrigo et al*., 2008b]. Both the sediment $CaCO_3$ and PP data sets were projected onto the bathymetric grid provided by *Timmermann et al*. [2010].

[10] As expected from the competing effects of PP on $CaCO_3$ production and dissolution (see Introduction), there is an optimum value of surface ocean PP where $CaCO_3$ content is maximal; this is elaborated in Figure 1. At PP levels below the optimum, $CaCO_3$ content decreases due to nutrient or food limitation of planktonic and benthic carbonate producers. Sediment $CaCO_3$ content is maximal at pelagic PP levels of 5 to 20 g C m^{-2} yr^{-1}. When PP exceeds the optimum value, $CaCO_3$ content decreases most probably due to carbonate dissolution in the sediments driven by oxic respiration and CO_2 production.

[11] In a first approach, all $CaCO_3$ data were fitted to a Gaussian distribution plus constant background value with upper ocean PP as an independent variable:

$$\mathrm{CaCO_3}\ (\%) = A_i \cdot \exp\left[-\frac{(\mathrm{PP}\ (g\ m^{-2}\ \mathrm{yr}^{-1}) - \mu_i)^2}{2\cdot\sigma_i^2}\right] + B_i, \quad (1)$$

where $CaCO_3$ (%) is the weight percentage of $CaCO_3$ in the dried sediment, and the parameters A_i (magnitude), μ_i (mean), σ_i (variance), and B_i (background value) were estimated using least squares regression.

[12] In a second approach, we took into account the water depth dependence of $CaCO_3$ content, as found in *Hauck et al*. [2012], and calculated individual fits for four

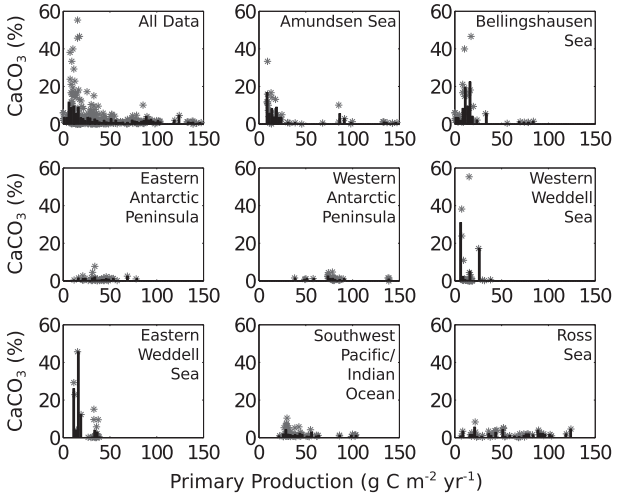

Figure 1. $CaCO_3$ versus primary production data for all shelf regions together (upper left) and the different shelf regions separately (name of region indicated in the diagram). Asterisks are original data; bars show means within 2.5 g C m^{-2} yr^{-1} bins.

water depth ranges: 0 to 250, 250 to 600, 600 to 900, and 900 to 1000 m. All fits were in the form of a Gaussian distribution plus a constant, as in equation (1). The estimated parameters A_i, B_i, μ_i, and σ_i, and their confidence intervals are listed in Table 1, and the resulting fits are shown in Figures 2 and 3.

[13] An ensemble of quantitative metrics (Table 2) was used to describe the goodness of fit, as recommended by *Stow et al*. [2009]. The correlation coefficient (r) describes to which extent model and observations vary together. A value close to 1 indicates that they show the same pattern of variation, and a negative value indicates inverse correlation. The root mean squared error (RMSE), average error (AE), and average absolute error (AAE) are all measures of the misfit, or in other words, of how far the predictions are away from the observations in the variable space. While the AE considers the sign of the discrepancy, and positive and negative discrepancies can average out, RMSE and AAE rather evaluate the magnitude of the offsets. Ideally, they would all be close to zero. The reliability index (RI),

$$\mathrm{RI} = exp\sqrt{\frac{1}{n}\sum_{i=1}^{n}\left(log\frac{O_i}{P_i}\right)^2}, \qquad (2)$$

with O_i being the observations, P_i the predictions, and n the number of data points, gives a multiplicative measure of the discrepancies between predictions and observations. An RI close to 1 would be ideal, RI = 2 indicates that the observations and predictions are, on average, a factor of 2 different. The modeling efficiency (MEF),

$$\mathrm{MEF} = \frac{\left(\sum_{i=1}^{n}(O_i-\bar{O})^2 - \sum_{i=1}^{n}(P_i-\bar{P})^2\right)}{\sum_{i=1}^{n}(O_i-\bar{O})^2}, \qquad (3)$$

is a measure of how much better or worse the predictions are compared to the mean of the observations. A MEF of 0 indicates that the model is only as good as the average of the observations; at a MEF less than 0, the model predictions are worse than the average of the observations, and at a MEF of 1, the model would exactly predict the observations [*Stow et al*., 2009].

[14] In the following section, where we compare observations to predictions, the observation is the mean $CaCO_3$ content grouped within a 2.5 g C m^{-2} yr^{-1} PP bin as in Figures 2 and 3. The statistical measures (Table 2) describing the discrepancies between observations and predictions (AAE and RMSE) for the depth-independent fit are at the lower end of those for the depth-dependent ones. The quantities describing the goodness of fit, including the correlation coefficient

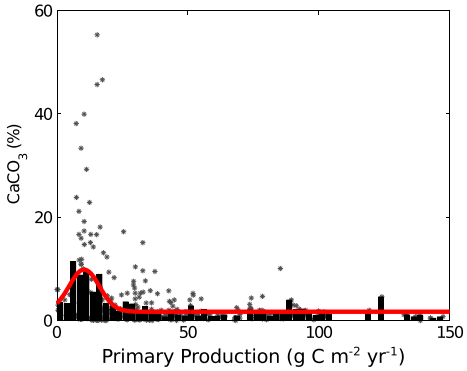

Figure 2. Fit to all data. Asterisks are original data; bars show means within 2.5 g C m^{-2} yr^{-1} bins. Red line shows fit to a Gaussian distribution plus constant background (equation (1) and Table 1).

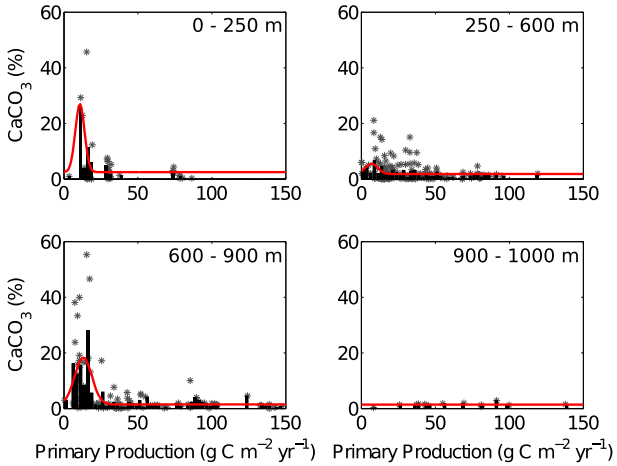

Figure 3. Fit within different depth ranges as indicated within the diagrams (0–250 m, 250–600 m, 600–900 m, 900–1000 m). Asterisks are original data; bars show means within 2.5 g C m^{-2} yr^{-1} bins. Red line shows fit to a Gaussian distribution plus constant background (equation (1) and Table 1).

Table 1. Estimated Parameters, Their 95% Confidence Intervals and Number of Observations (n) Derived to Describe $CaCO_3$ as a Function of Primary Production (See Equation (1) and Figures 2 and 3) Using a Depth-Independent Fit and Using Four Fits for Four Depth Compartments: 0 to 250, 250 to 600, 600 to 900, and 900 to 1000 m

Depth Range (m)	A_i	μ_i	σ_i	B_i	n
Depth-independent fit					
0–1000	8.16 ± 2.00	10.41 ± 2.24	5.77 ± 2.37	1.71 ± 0.78	358
Depth-dependent fits					
0–250	24.52 ± 17.58	10.79 ± 5.07	3.10 ± 3.04	2.52 ± 3.07	35
250–600	3.70 ± 2.19	6.88 ± 2.86	4.17 ± 2.64	1.84 ± 0.54	184
600–900	16.79 ± 4.59	13.07 ± 1.88	5.78 ± 2.55	1.48 ± 1.57	125
900–1000	—	—	—	1.43 ± 0.35	14

Table 2. Statistics for Fits

Depth range (m)	*r*	RMSE	AE	AAE	RI	MEF
Depth-independent fit						
0–1000	0.86	1.3	–0.82	0.93	1.68	0.74
Depth-dependent fits						
0–250	0.84	3.90	–0.54	3.09	3.14	0.69
250–600	0.58	1.13	–0.25	0.91	1.85	0.28
600–900	0.81	3.12	–0.03	1.82	2.02	0.65
900–1000	—	0.59	0.05	0.42	1.64	-0.01

AAE, average absolute error; AE, average error or bias; MEF, modelling efficiency; *r*, correlation coefficient; RI, reliability index; RMSE, root mean squared error. See *Stow et al*. [2009] and text for further explanation.

and MEF, are accordingly higher for the depth-independent fit than for any of the depth-dependent fits. The MEF for the depth-dependent fit of the depth range 900 to 1000 m is zero, as the model is basically the observation average. The depth-independent fit predicts the observations within a factor of 1.68 (RI), which is as reliable as the depth-dependent fit for the 900 to 1000 m depth range (RI = 1.64) and more reliable than for the 0 to 250, 250 to 600, and 600 to 900 m depth ranges. All univariate goodness-of-fit statistics show that the depth-independent fit is a better predictor of $CaCO_3$ content as a function of PP.

[15] There are two caveats of the depth-dependent parameterization. One is that the number of data points available for the fit is strongly reduced by splitting the data set into four depth compartments, which negatively affects the quality of the fits. The second source of error is the uncertainty associated with the topography product of *Timmermann et al*. [2010]. Although this is a high-quality product with errors as low as 2% of the water depth close to ship tracks, the error is higher where data were extrapolated, with an upper limit being defined as 250 m. At the boundary between depth compartments, errors arise when locations are grouped into the wrong depth compartment where $CaCO_3$ content predictions differ. However, the fits for the depth ranges where high $CaCO_3$ contents were found (0–250 m and 600–900 m) are only slightly inferior in terms of correlation coefficient and MEF. It is therefore reasonable to further evaluate both fitting procedures.

[16] The $CaCO_3$ distributions in the different shelf regions all peak at similar PP values (Figure 1), so that no bias is expected when applying a single fit to the entire circum-Antarctic data set.

[17] One drawback of both parameterizations is that the sharp increase of $CaCO_3$ at PP levels of 5 g C m^{-2} yr^{-1} is not well reproduced by the Gaussian fit (Figures 2 and 3). For the depth-independent parameterization, $CaCO_3$ levels are overestimated for PP levels of 0 to 5 g C m^{-2} yr^{-1} and underestimated at 5 to 7.5 g C m^{-2} yr^{-1}. The latter underestimation is also observed in the depth-dependent parameterization for the 600 to 900 m range.

[18] The depth-independent parameterization does not allow $CaCO_3$ content greater than 10%; however, these high values are sparse in the observations, and averaging the $CaCO_3$ content over PP ranges of 2.5 g C m^{-2} yr^{-1} yields no mean $CaCO_3$ of more than 12%.

[19] Two circum-Antarctic maps of $CaCO_3$ (weight %) were produced by applying equation (1) to all PP data at water depths shallower than 1000 m and south of 60°S with either the depth-independent or depth-dependent sets of parameters. $CaCO_3$ was calculated at a latitudinal and longitudinal resolution of 0.25° × 0.25°. To account for the fact that organic material and carbonate components produced by organisms feeding on the phytoplankton do not always sink to the seafloor at the exact position where they were produced because of advection by currents, we use the mean PP in a 0.5° × 0.5° box around each position as input PP in equation (1). Averaging the PP data from a 4 km resolution onto a coarser scale also further reduces its uncertainty.

3. Results and Discussion

3.1. Evaluation of $CaCO_3$ Maps

[20] The predicted $CaCO_3$ distributions for both the depth-dependent and depth-independent parameterizations are presented in Figure 4. As prescribed by the parameterization, $CaCO_3$ sediments do not appear in the high-production regions around the western Antarctic Peninsula, in the Ross Sea and in Prydz Bay. High $CaCO_3$ content appears at the outer Amundsen and Bellingshausen and southwestern Weddell seas, and on the narrow shelves of the eastern Weddell Sea and the swP/IO sectors of the Southern Ocean.

[21] The two parameterizations differ in the magnitude of $CaCO_3$ accumulations at those places where significant amounts are predicted, e.g., in the Amundsen and Bellingshausen seas, the southwestern Weddell Sea, and the southeastern Antarctic Peninsula. The depth-independent parameterization produces more regions with values between 7% and the maximum value of 10%. The map generated using the depth-dependent parameterization displays only few locations with more than 7% $CaCO_3$, but peak values go up to 27% (Figure 3).

[22] The depth-independent parameterization produces large areas with the maximum $CaCO_3$ content on the southeastern Antarctic Peninsula and southwestern Weddell Sea shelves. Like in the Bellingshausen and Amundsen seas, the depth-dependent parameterization shows a similar pattern as the depth-independent parameterization, but generally with lower values. The environmental setting in the southwestern Weddell Sea is very similar to the one in the Amundsen and Bellingshausen seas where the broad and deep shelves are covered with sea ice for most of the year. High sedimentary $CaCO_3$ content in the Amundsen and Bellingshausen seas was explained by high numbers of the planktonic foraminifera *Neogloboquadrina pachyderma* from the water column and the sea ice, which may also be concentrated by winnowing of silt and clay [*Hillenbrand et al*., 2003; *Hauck et al*., 2012]. While only parts of the western Weddell Sea were covered by the data compilation of *Hauck et al*. [2012], a high

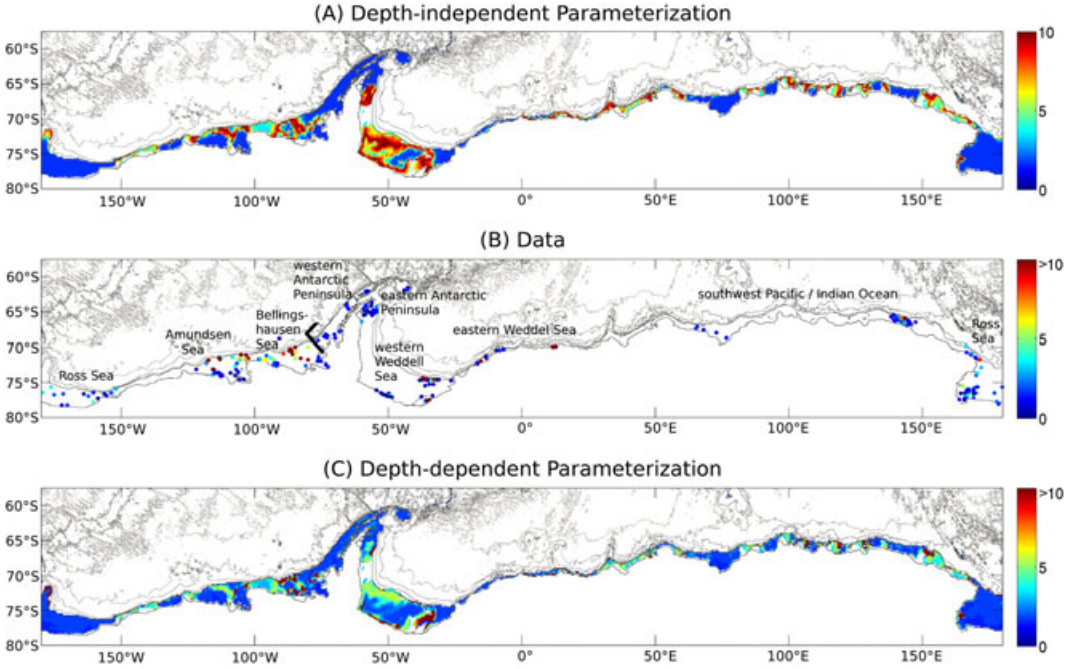

Figure 4. $CaCO_3$ (% dry weight) maps produced with PP-$CaCO_3$-parameterization (a) map of predicted $CaCO_3$ (%) data with depth-independent parameterization, (b) $CaCO_3$ (%) data from *Hauck et al*. [2012], (c) map of predicted $CaCO_3$ (%) data with depth-dependent parameterization. Note that (b) and (c) do not show the full range but are cut off at 10% for better comparability with (a).

number of planktonic calcareous foraminifera was found on the outer shelf and slope of the southwestern Weddell Sea and eastern Antarctic Peninsula south of 65°S by *Anderson* [1975]. Assuming that a high ratio of calcareous to arenaceous foraminifera,as found by *Anderson* [1975], corresponds to high $CaCO_3$ content, the calculation of high $CaCO_3$ content on the outer shelves of the southeastern Antarctic Peninsula and southwestern Weddell Sea appears to be reasonable. The band of high values on the inner shelf along the coast of the southwestern Weddell Sea does not correspond with observations (compare Figure 4b) and is probably spurious. Within the period considered (1997–2006), the polynya on the inner southwestern Weddell Sea shelf was open for only 2 years. The time series is probably too short to capture the true mean PP in this area.

[23] To complete the evaluation, we compare predicted to observed $CaCO_3$ content at each sample location. As the $CaCO_3$ distribution is very patchy, we calculate the mean $CaCO_3$ in a 100 km radius around each measured or modeled data point. We compare these smoothed data sets and also the average measured and modeled $CaCO_3$ concentration in the different regions (Figure 5). Although these averaging or smoothing procedures are needed, they also have caveats. The mean of the measurements can only be calculated where data for averaging is available and is biased by the clustering of data points in certain regions and by the sparseness of data in others. Therefore, it is hard to judge the skill of the model based on this comparison, and we refer to the earlier discussion of the produced maps. Clearly, the modeled $CaCO_3$ content in the swP/IO, eastern Antarctic Peninsula, and western Weddell Sea regions is higher than observed, due to the fact that areas with high values were calculated for former data gaps. This is more pronounced in the depth-independent parameterization. In contrast, the model suggests that areas with high $CaCO_3$ content were over-represented in the Amundsen Sea, Bellingshausen Sea, and eastern Weddell Sea regions.

[24] The mapping procedure fills in situ data gaps in the swP/IO sectors of the Antarctic shelves. As most swP/IO data from *Hauck et al*. [2012] were from locations with relatively high PP levels (Figure 1), the mapping procedure reveals possible $CaCO_3$ accumulation sites. It is now possible to split the swP/IO region into the highly productive Prydz Bay [*Arrigo et al*., 2008b] and the remainder of the

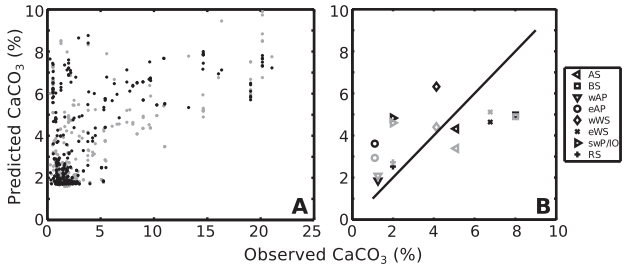

Figure 5. Comparison of observed versus predicted $CaCO_3$ (% dry weight) for the depth-independent (black) and depth-dependent (grey) parameterizations. (a) Observations and predictions were smoothed by averaging over a 100 km radius around each measured or predicted data point. (b) Regional averages were calculated for the data and predictions for the Amundsen Sea (AS), Bellingshausen Sea (BS), western Antarctic Peninsula (wAP), eastern Antarctic Peninsula (eAP), western Weddell Sea (wWS), eastern Weddell Sea (eWS), southwest Pacific/Indian Ocean (swP/IO), and Ross Sea (RS) regions. Black line shows the one-to-one line.

region. In Prydz Bay, oxic remineralization of organic material drives dissolution of carbonates in the sediments. The remainder of the area has a similar setting as the eastern Weddell Sea, with shallow shelves and limited sea-ice cover. We may therefore expect that carbonates are preserved at shallow depths and that both planktonic and benthic organisms contribute to the $CaCO_3$ production. The swP/IO remains a possible accumulation site for pteropods, as hypothesized by [*Hauck et al*., 2012], because it fulfills the requirements for $CaCO_3$ preservation (shallow shelf, average PP, high pteropod density reported by *Hunt et al*. [2008]). The identification of possible $CaCO_3$ accumulation sites in the swP/IO region suggests that this hypothesis may be valid. However, observations are needed to prove or disprove the hypothesis.

3.2. Proposed Relationship Between PP and Sedimentary $CaCO_3$

[25] Our study aims to estimate the amount of sedimentary $CaCO_3$ available for dissolution. Motivated by the hypothesis that PP controls $CaCO_3$ production in the water column and its dissolution due to metabolic-CO_2 release in the sediments, we derived an empirical parameterization between sedimentary $CaCO_3$ and PP. Clearly, this is a simplification of a chain of processes in the real world. In this section, we explain and discuss the implicit assumptions. However, more research, particularly highly resolved time series of flux measurements, would be necessary to quantify or mechanistically explain all these processes. This is beyond the scope of our study. We propose that: (1) satellite-derived ocean color measurements can be used to calculate PP, (2) the rain of organic carbon (C_{org}) to the sediments is linked to export production and export production to PP, (3) $CaCO_3$ production is linked to PP and $CaCO_3$ flux to C_{org} flux, (4) $CaCO_3$ rain to the sediments correlates with $CaCO_3$ production and export, (5) organic carbon remineralization in the sediments correlates with C_{org} rain to the sediments, and (6) contemporary $CaCO_3$ dissolution is related to organic carbon remineralization in the sediments (see Figure 6 for a scheme of the C_{org} and $CaCO_3$ cycles).

[26] 1. The algorithm to derive PP from ocean color was described in detail by *Arrigo et al*. [2008b] together with a thorough error analysis.

[27] 2. We assume that the C_{org} rain to the seafloor is a function of export production, which, in turn, is assumed to be a function of PP. The ratio of export production to PP has been empirically parameterized in various ways, as the f-ratio [assuming new production/total production = export production/total production; *Laws et al*., 2000], the ThE ratio [^{234}Th-derived export/PP; Henson *et al*., 2011] or the pe-ratio (particle export/PP; *Dunne et al*., 2005]. All these parameterizations, being functions of temperature [*Laws et al*., 2000; *Henson et al*., 2011] and PP [*Dunne et al*., 2005], have in common that more C_{org} is exported when PP increases. Once exported out of the euphotic zone, the downward C_{org} flux decreases with depth, which has been established as the "Martin curve" [*Martin et al*., 1987, Figure 6, right panel]. The exact parameters for the Martin curve are under discussion, and the percentage of C_{org} that reaches the seafloor varies regionally [e.g., *Henson et al*., 2011], but the crucial point is that C_{org} reaching the seafloor can be expressed as a percentage of the export production. The basic shape of the Martin curve is widely accepted [*Boyd and Trull*, 2007; *Berelson*, 2001; *Berelson et al*., 2007]. For this regional study, constrained to the Antarctic shelves, we expect that an increase in PP goes along with an increase in C_{org} export and rain to the seafloor.

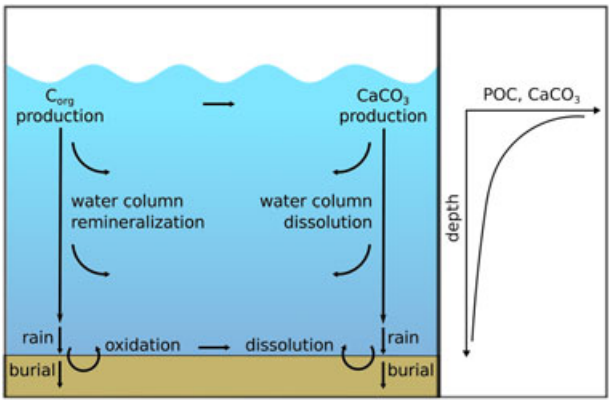

Figure 6. Schematic illustration of $CaCO_3$ and C_{org} cycles. The empirically derived parameterization between PP and $CaCO_3$ assumes that more $CaCO_3$ is produced when more C_{org} is produced, that C_{org} and $CaCO_3$ rain to the sediments are functions of the C_{org} and $CaCO_3$ production (as the particle flux decreases with depth as shown in the right panel), and that oxidation of C_{org} in the sediments may lead to $CaCO_3$ dissolution.

[28] 3. Assuming a relationship between $CaCO_3$ production and PP is equivalent to assuming a relationship between $CaCO_3$ and C_{org} rain to the seafloor (given assumptions 2 and 4). As $CaCO_3$ is produced by organisms, it is by definition coupled to PP. A large portion of C_{org} is remineralized within the water column, and a smaller percentage of C_{org} than of $CaCO_3$ reaches the seafloor. As a first approximation, we assume that $CaCO_3$ production increases when PP increases, at least at low PP levels. Sediment trap data from the Antarctic shelves (water depths up to 1000 m; data from *Accornero et al*. [2003] and *Collier et al*. [2000]) reveal a strong correlation between $CaCO_3$ and C_{org} fluxes (correlation coefficient 0.93; see Figure 7b). Even in the wider region south of 60°S [data from *Accornero et al*., 2003; *Collier et al*., 2000; *Honjo et al*., 2000; *Wefer and Fischer*, 1991; *Wefer et al*., 1989; *Wefer et al*., 1988; *Pilskaln et al*., 2004], $CaCO_3$ and C_{org} fluxes are correlated with a correlation coefficient of 0.8 (Figure 7a).

[29] 4. Along the lines of assumption 2, we assume that the flux of $CaCO_3$ is a function of $CaCO_3$ production and that it decreases with depth. In this regional study, constrained to the Antarctic shelves, we expect that the $CaCO_3$ flux, relative to $CaCO_3$ export out of the mixed layer, follows a uniform profile and that more $CaCO_3$ reaches the seafloor when more $CaCO_3$ is produced. This is in line with widely used estimates of increasing $CaCO_3$ dissolution with depth [e.g., *Chung et al*., 2003] and with the decrease of the calcite and aragonite saturation states with increasing pressure [e.g., *Zeebe and Wolf-Gladrow*, 2001].

[30] 5. We assume that the amount of organic carbon that is remineralized in the sediments (and accordingly

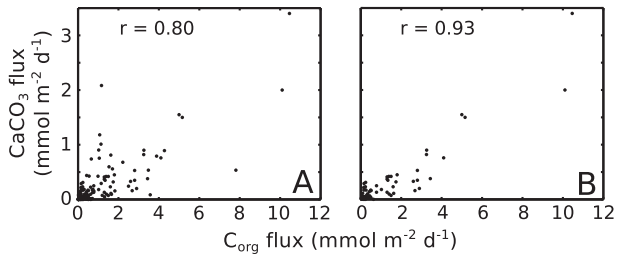

Figure 7. $CaCO_3$ flux versus particulate organic carbon flux from Southern Ocean sediment trap studies. (a) Sediment traps from all water depths south of 60°S considered. (b) Only sediment traps from the Antarctic shelves with water depths up to 1000 m considered. Correlation coefficients (r) indicate strong correlation of particulate organic carbon and $CaCO_3$ flux. See text for data sources.

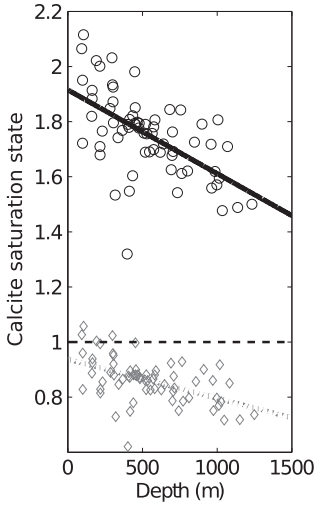

Figure 8. The calcite saturation state in the bottom water on the Antarctic shelf (black symbols and line) as calculated from GLODAP and CARINA data [see *Hauck et al*., 2012, for filtering procedure]. The grey symbols and dashed regression line were calculated with a presumed metabolic DIC increase of 100 μmol kg^{-1} in the pore water as estimated from oxygen profiles in the high-production regions of the Antarctic shelf [*Sachs et al*., 2009].

the oxygen consumption and CO_2 production) is related to the C_{org} rain to the sediment that is, in turn, related to PP via relationship (2). It follows that more oxic remineralization of C_{org} occurs in regions of high PP, as shown by *Sachs et al*. [2009].

[31] 6. Metabolic CO_2 release due to oxic remineralization of C_{org} leads to $CaCO_3$ dissolution [*Berger*, 1970; *Archer*, 1996; *Martin and Sayles*, 2003]. This is in line with the observation that no significant accumulation of $CaCO_3$ was found in the high-production regions of the Southern Ocean, such as Prydz Bay, the western Antarctic Peninsula, and the Ross Sea [*Hauck et al*., 2012]. These authors also used oxygen pore water profiles from *Sachs et al*. [2009] to explain that aragonite cannot be preserved in Antarctic shelf sediments. In this study, we add to this by calculating how much the calcite saturation state can change as a result of metabolic CO_2 production (Figure 8). Oxygen profiles from the Antarctic shelf [*Sachs et al*., 2009] suggest that in the high-production regions, DIC can increase by as much as 100 to 200 μmol kg^{-1} due to oxic remineralization of organic matter in the first centimeter of the sediment. Recalculating the calcite saturation state for the pore waters using a DIC increase of 100 μmol kg^{-1} leads to calcite undersaturation at all depths, and therefore to metabolic-CO_2–driven dissolution of $CaCO_3$. This supports our proposed relationships (2) and (5). As an additional constraint, we plot $CaCO_3$ versus C_{org} content (Figure 9). There is an indication of more $CaCO_3$ at low C_{org}. This should, however, be treated with caution, as it is unknown how much C_{org} has been oxidized already.

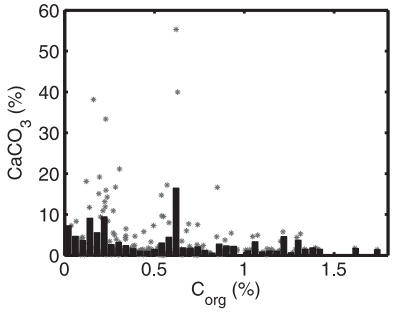

Figure 9. Sedimentary $CaCO_3$ versus sedimentary organic carbon content [*Hauck et al*., 2012]. Asterisks show original data; black bars show average $CaCO_3$ (%) within 0.04% C_{org} bins. There is an indication that high $CaCO_3$ contents occur at low C_{org} levels; however, this disregards how much C_{org} has been oxidized already.

3.3. $CaCO_3$ Reservoir

[32] One of the main aims is to quantify the total inventory of $CaCO_3$ on Antarctic continental shelves. Quantification is based on the charts with predicted $CaCO_3$ content (Figure 4). Further, we follow the procedure of *Archer* [1996]. We assume that the inventory of $CaCO_3$, which is capable of buffering anthropogenic carbon, is formed by the upper 10 cm of the sediments. First, $CaCO_3$ (%) data were converted to the $CaCO_3$ content in the 10 cm surface layer (g km^{-2}) using the following equation:

$$\mathrm{CaCO_3}\ \left(g\ \mathrm{km^{-2}}\right) = \frac{\mathrm{CaCO_3}(\%)}{100} \cdot \rho \cdot (1-\varphi) \cdot d \cdot f, \qquad (4)$$

where the average porosity (φ) of the top 10 cm of the sediment is based on the percentage of $CaCO_3$ [*Archer*, 1996; *DeMenocal et al*., 1993]. Calculated porosities range from 0.845 to 0.860 with a mean of 0.857 for the depth-independent parameterization and from 0.812 to 0.860 with a mean of 0.858 for the depth-dependent parameterization. We use an average grain density (ρ) of 2.5 g cm^{-3} and assume that the $CaCO_3$ content is constant in the upper 10 cm (d) of the sediment, reflecting the bioturbated layer in which $CaCO_3$ can dissolve [*Archer*, 1996; *Berger and*

Killingley, 1982; *Boudreau*, 1994; *Martin and Sayles*, 2003]. The factor $f = 10^{-10}$ converts from units of g cm^{-2} to g km^{-2}.

[33] The assumptions on porosity and on bioturbation depth induce some additional uncertainty in the inventory estimate as they define the mass of the sediment that is in contact with the pore water. The inventory of $CaCO_3$ (as obtained by multiplication of the total mass in each grid box with the relative contribution of $CaCO_3$, in units of weight %) is assumed to be available for dissolution when in contact with a calcite undersaturated water column due to anthropogenic carbon uptake. For the sake of consistency and due to the lack of better constraints for the circum-Antarctic shelf environment, we follow the approach of *Archer* [1996] as described in equation (4). In reality, the porosity of Antarctic shelf sediments might follow a somewhat different relationship than the one developed by *DeMenocal et al*. [1993] and *Archer* [1996] for deep-sea sediments. However, a consistent circum-Antarctic assessment for the porosity profile in the upper 10 cm of the sediment is not available, nor is there a circumpolar map of bioturbation depths, disturbance by iceberg scouring, or percentage of area covered by macrozoobenthos, which might also affect the total $CaCO_3$ inventory.

[34] In the second step, $CaCO_3$ (g km^{-2}) was integrated over the area of the entire Antarctic continental shelf (4.4×10^6 km^2). The inventory calculated with the depth-independent parameterization amounts to 4.3 Pg $CaCO_3$ or 0.52 Pg C, whereas the depth-dependent parameterization yields 4.0 Pg $CaCO_3$ or 0.48 Pg C. The spatial dissimilarities between the two different parameterizations level out when integrating over the whole Antarctic shelf. We consider all uncertainties to be accounted for by applying the two different fitting procedures. A back-of-the-envelope estimate to test whether these numbers are in a reasonable range can be done by calculating the inventories separately in the different shelf regions (Table 3), based on the means of the observations, the assumptions on porosity and bioturbation depth, and the area of the regions (Amundsen Sea, Bellingshausen Sea, western and eastern Antarctic Peninsula, western and eastern Weddell Sea, swP/IO, and Ross Sea). Summing up these independent estimates leads to a total of 4.9 Pg $CaCO_3$ or 0.59 Pg C. This is in the same range as the PP and depth-based estimates, and confirms that our method is valid. However, given that the samples were not randomly distributed and large data gaps exist, this simple estimate alone would not be trustworthy. The interpolation procedure we presented fills data gaps based on environmental conditions, it can be used to produce maps, and it is more appropriate to calculate an inventory, even though it also has drawbacks (see section 3.1).

[35] Thus, the total inorganic carbon content able to buffer anthropogenic increases in CO_2 amounts to 0.5 Pg C or 113 g C m^{-2}. The latter value is more than a factor of 100 smaller than the global average amount of biologically produced $CaCO_3$ in shallow water sediments (18×10^3 g C m^{-2} calculated from an estimate of 517 Pg C over an area of 28.3×10^6 km^2) [*Andersson et al*., 2003]. The dissimilarities between these estimates are mainly due to the different contents of $CaCO_3$ in the sediments. *Andersson et al*. [2003] assume 15% $CaCO_3$ in 95% of the sediment area and 80% $CaCO_3$ in the remaining 5%, which is much more than we found in Antarctic shelf sediments. However, their inventory is overestimated by defining the reactive sediment as a 1 m layer. In contrast, we use a reactive or bioturbated layer of 10 cm, in agreement with previous work [*Archer*, 1996; *Broecker and Takahashi*, 1977; *Peng et al*., 1977]. We do not consider exposure of $CaCO_3$ from underneath the bioturbated layer due to erosion. This is legitimate because with percentages of $CaCO_3$ of 10% or less, dissolution of $CaCO_3$ does not induce a significant mass loss. *Andersson et al*. [2003] could have considered erosion and subsequent entrainment of older $CaCO_3$ from below, but the assumption of a static sediment column thicker than the bioturbated layer was shown to overestimate the $CaCO_3$ inventory by a factor of 2 to 3 [*Archer*, 1996; *Sundquist*, 1985, and references therein].

[36] For comparison, the buffering capacity of global deep-sea sediments was estimated to be about 1600 Pg C by *Archer* [1996], which is a factor of 3 smaller than the estimate by *Broecker and Takahashi* [1977], who used a static sediment column. To obtain a truly global estimate for the inventory of erodible $CaCO_3$, a new data compilation would be needed to fill data gaps in shallow-water and polar regions from the *Archer* [1996] estimate.

[37] Although there may be uncertainties associated with the global shallow water reservoir, it is certain that the Antarctic reservoir is comparatively small. This suggests that the Antarctic shelves have a limited capacity for buffering anthropogenic increases in CO_2.

3.4. Buffering Capacity of Antarctic Shelf Carbonates

[38] The dissolution of $CaCO_3$ can be expressed by more than one reaction equation [e.g., *Hofmann et al*., 2010], for instance by

$$CaCO_3 + CO_2 + H_2O \rightarrow Ca^{2+} + 2\ HCO_3^- \quad (5)$$

or

$$CaCO_3 \rightarrow Ca^{2+} + CO_3^{2-}. \quad (6)$$

[39] All formulations have in common that the DIC pool and the total alkalinity (A_T) pool increase in the molar ratio of 1 to 2, i.e.,

Table 3. $CaCO_3$ Inventory Based on Regional Average $CaCO_3$ Concentrations

	AS	BS	wAP	eAP	wWS	eWS	swP/IO	RS	sum
$CaCO_3$ (%)	5.1	8.0	1.3	1.0	4.3	6.8	2.0	2.0	
Area (10^5 km^2)	3.35	3.16	2.88	2.69	7.50	1.91	9.88	1.04	
$CaCO_3$ (Pg)	0.62	0.96	0.13	0.09	1.18	0.48	0.69	0.73	4.90
C (Pg)	0.08	0.12	0.02	0.01	0.14	0.06	0.08	0.09	0.59

AS, Amundsen Sea; BS, Bellingshausen Sea; eAP, eastern Antarctic Peninsula; eWS, eastern Weddell Sea; swP/IO, southwest Pacific/Indian Ocean; wAP, western Antarctic Peninsula; wWS, western Weddell Sea.

$$\Delta A_T = 2\ \Delta DIC. \quad (7)$$

[40] This leads to a shift in carbonate equilibria, an increase of carbonate ions and a decrease of CO_2, enhancing the ability of the ocean to take up additional CO_2 from the atmosphere. Approximately 0.8 to 0.9 mol CO_2 is neutralized by dissolution of 1 mol $CaCO_3$ (the exact factor depends on DIC, A_T, T, and S; for details, see *Zeebe and Wolf-Gladrow* [2001]. The total amount of carbon that could be neutralized, i.e., taken up by the ocean without significant changes in pH and $CaCO_3$ saturation states, by the dissolution of the entire Antarctic shelf inventory is thus 0.4 to 0.45 Pg C. This estimate is of the same order of magnitude as most of the recent estimates for the Southern Ocean CO_2 uptake per year, e.g., 0.41 Pg C yr^{-1} south of 40°S [*Valsala and Maksyutov*, 2010], 0.3 Pg C yr^{-1} south of 44°S [*Gruber et al*., 2009; *Takahashi et al*., 2009, as recalculated by *Gruber et al*. [2009]], 0.05 Pg C yr^{-1} south of 50°S [*Takahashi et al*., 2009], and 0.4 Pg C yr^{-1} south of 50°S [*McNeil et al*., 2007].

[41] To compare the buffering capacity of the shelf sediments with observed anthropogenic CO_2 increases over the last few decades, the inventories need to be converted into the concentration of CO_2 that can be buffered per water parcel. This requires taking the volume of the overlying water into consideration. If we were to consider only the volume above the shelves (1.8×10^{15} m^3) and instantaneous dissolution of the sediment $CaCO_3$, approximately 14 to 18 μmol kg^{-1} CO_2 could be buffered per kilogram of seawater. This is a significant number, corresponding to the increase in anthropogenic carbon over at least two decades on the Antarctic shelf [*Hauck et al*., 2010]. However, due to the slow rate of dissolution at a saturation state close to 1 [*Keir*, 1980; *Hales and Emerson*, 1997] and mixing with neighboring water masses, values this high will not be reached. As a second example, we assume that the dissolved carbonate from the shelf would be mixed into adjacent waters soon after release. Hence, converting the $CaCO_3$ inventory to concentrations requires a volume larger than the water column above the shelf to be taken into account. Using the volume of the Southern Ocean south of 60°S (7×10^{16} m^3) to calculate a concentration of anthropogenic CO_2 that can be buffered by dissolution of $CaCO_3$, we calculate that only approximately 0.5 μmol CO_2 could be buffered per kilogram of seawater, before all carbonates in the bioturbated layer on the Antarctic shelf have been dissolved. The true value depends on the $CaCO_3$ dissolution rate, which differs by several orders of magnitude between laboratory experiments and field data [*Hales and Emerson*, 1997], the mixing of the overlying water, and will probably be below the detection limit.

4. Conclusions

[42] The sedimentary carbonate content of the Antarctic shelf is mainly determined by primary production (PP) in the overlying water column. The $CaCO_3$ content first increases with increasing PP, eventually reaching an optimum value, but then decreases with further increasing PP.

[43] The relationship between PP and $CaCO_3$ content can be used to estimate the $CaCO_3$ content in regions where no in situ data are available. The buffering capacity of carbonates in Antarctic shelf sediments is too small to delay ocean acidification. This is a surprising outcome, considering the extent of the global abundance of carbonates in shelf sediments. As acidification proceeds, carbonates in the sediments will likely disappear in the end without significantly enhancing the buffering capacity of the ocean.

[44] As polar surface waters are very sensitive to acidification, our results imply that the situation for those sensitive waters is worse than previously thought. The uptake of anthropogenic CO_2 will in the near future cause undersaturation of aragonite [*Orr et al*., 2005; *González-Dávila et al*., 2011; *McNeil and Matear*, 2008], which will hamper the formation of carbonate shells in organisms like pteropods, with possible aggravating impact on the Antarctic ecosystem. The sediments will not be able to function as a buffer to stop or delay this trend.

[45] **Acknowledgments.** This article is a contribution to the German project Biological Impacts of Ocean Acidification (BIOACID), funded by the Federal Ministry of Education and Research (BMBF, FKZ 03F0608B).

References

Accornero, A., C. Manno, F. Esposito, and M. C. Gambi (2003), The vertical flux of particulate matter in the polynya of Terra Nova Bay. Part II: Biological components, *Antarct. Sci.*, *15*, 175–188, doi:10.1017/S0954102003001214.

Anderson, J. B. (1975), Factors controlling $CaCO_3$ dissolution in the Weddell Sea from foraminiferal distribution patterns, *Mar. Geol.*, *19*, 315–332, doi:10.1016/0025-3227(75)90083-3.

Andersson, A. J., F. T. Mackenzie, and L. M. Ver (2003), Solution of shallow-water carbonates: An insignificant buffer against rising atmospheric CO_2, *Geology*, *31*, 513–516.

Archer, D. (1996), An atlas of the distribution of calcium carbonate in sediments of the deep-sea, *Global Biogeochem. Cycles*, *10*, 159–174, doi:10.1029/95GB03016.

Arrigo, K. R., G. van Dijken, and M. Long (2008a), Coastal Southern Ocean: A strong anthropogenic CO_2 sink, *Geophys. Res. Lett.*, *35*, L21602, doi:10.1029/2008GL035624.

Arrigo, K. R., G. L. van Dijken, and S. Bushinsky (2008b), Primary production in the Southern Ocean, 1997-2006, *J. Geophys. Res.*, *113*, C08004, doi:10.1029/2007JC004551.

Berelson, W. M. (2001), The flux of Particulate Organic Carbon into the ocean interior: A comparison of four U.S.-JGOFS regional studies, *Oceanography*, *14*, 59–67.

Berelson, W. M., W. M. Balch, R. Najjar, R. A. Feely, C. Sabine, and K. Lee (2007), Relating estimates of $CaCO_3$ production, export, and dissolution in the water column to measurements of $CaCO_3$ rain into sediment traps and dissolution on the sea floor: A revised global carbonate budget, *Global Biogeochem. Cycles*, *21*, *GB1024*, doi:10.1029/2006GB002803.

Berger, W. H. (1970), Planktonic Foraminifera: Selective solution and the lysocline, *Mar. Geol.*, *8*, 111–138, doi:10.1016/0025-3227(70)90001-0.

Berger, W. H., and J. S. Killingley (1982), Box cores from the equatorial Pacific: ^{14}C sedimentation rates and benthic mixing, *Mar. Geol.*, *45*, 93–125, doi:10.1016/0025-3227(82)90182-7.

Boudreau, B. P. (1994), Is burial velocity a master parameter for bioturbation?, *Geochim. Cosmochim. Acta*, *58*, 1243–1249, doi:10.1016/0016-7037(94)90378-6.

Boyd, P. W., and T. W. Trull (2007), Understanding the export of biogenic particles in oceanic waters: Is there consensus?, *Prog. Oceanogr.*, *72*, 276–312, doi:10.1016/j.pocean.2006.10.007.

Broecker, W. S., and T. Takahashi (1977), Neutralization of fossil fuel CO_2 by marine calcium carbonate, in *The Fate of Fossil Fuel CO_2 in the Oceans*, edited by N. R. Anderson and A. Malahoff, pp. 213–241, Plenum, New York.

Chung, S.-N., K. Lee, R. A. Feely, C. L. Sabine, F. J. Millero, R. Wanninkhof, J. L. Bullister, R. M. Key, and T.-H. Peng (2003), Calcium carbonate budget in the Atlantic Ocean based on water column inorganic carbon chemistry, *Global Biogeochem. Cycles*, *17*, 1093, doi:10.1029/2002GB002001.

Collier, R., J. Dymond, S. Honjo, S. Manganini, R. Francois, and R. Dunbar (2000), The vertical flux of biogenic and lithogenic material in the Ross Sea: moored sediment trap observations 1996-1998, *Deep-Sea Res. II*, *47*, 3491–3520, doi:10.1016/S0967-0645(00)00076-X.

DeMenocal, P. B., W. F. Ruddiman, and E. M. Pokras (1993), Influences of high- and low-latitude processes on African terrestrial climate: Pleistocene eolian records from equatorial Atlantic Ocean Drilling Program site 663, *Paleoceanography*, *8*, 209–242, doi:10.1029/93PA02688.

Dunne, J. P., R. A. Armstrong, A. Gnanadesikan, and J. L. Sarmiento (2005), Empirical and mechanistic models for the particle export ratio, *Global Biogeochem. Cycles*, *19*, GB4026, doi:10.1029/2004GB002390.

Friedlingstein, P., R. A. Houghton, G. Marland, J. Hackler, T. A. Boden, T. J. Conway, J. G. Canadell, M. R. Raupach, P. Ciais, and C. Le Quéré (2010), Update on CO_2 emissions, *Nat. Geosci.*, *3*, 811–812, doi:10.1038/ngeo1022.

Global Carbon Project (2010), Global Carbon Project: Carbon budget and trends 2009, released 21 November 2010. [Available at: http://www.globalcarbonproject.org/carbonbudget.]

González-Dávila, M., J. M. Santana-Casiano, R. M. Fine, B. Happell, B. Delille, and S. Speich (2011), Carbonate system buffering in the water masses of the Southwest Atlantic sector of the Southern Ocean during February–March 2008, *Biogeosciences*, *8*, 1401–1413, doi:10.5194/bg-8-1401-2011.

Gruber, N., et al. (2009), Oceanic sources, sinks, and transport of atmospheric CO_2, *Global Biogeochem. Cycles*, *23*, GB1005, doi:10.1029/2008GB003349.

Hales, B., and S. Emerson (1997), Evidence in support of first-order dissolution kinetics of calcite in seawater, *Earth Planet. Sci. Lett.*, *148*, 317–327, doi:10.1016/S0012-821X(97)00017-4.

Hauck, J., D. Gerdes, C.-D. Hillenbrand, M. Hoppema, G. Kuhn, G. Nehrke, C. Völker, and D. A. Wolf-Gladrow (2012), Distribution and mineralogy of carbonate sediments on Antarctic shelves, *J. Mar. Syst.*, *90*, 77–87, doi:10.1016/j.jmarsys.2011.09.005.

Hauck, J., M. Hoppema, R. G. J. Bellerby, C. Völker, and D. Wolf-Gladrow (2010), Data-based estimation of anthropogenic carbon and acidification in the Weddell Sea on a decadal timescale, *J. Geophys. Res.*, *115*, *C03004*, doi:10.1029/2009JC005479.

Henson, S. A., R. Sanders, E. Madsen, P. J. Morris, F. Le Moigne, and G. D. Quartly (2011), A reduced estimate of the strength of the ocean's biological carbon pump, *Geophys. Res. Lett.*, *38*, L04606, doi:10.1029/2011GL046735.

Hillenbrand, C.-D., H. Grobe, B. Diekmann, G. Kuhn, and D. K. Fütterer (2003), Distribution of clay minerals and proxies for productivity in surface sediments of the Bellingshausen and Amundsen seas (West Antarctica)—relation to modern environmental conditions, *Mar. Geol.*, *193*, 253–271, doi:10.1016/S0025-3227(02)00659-X.

Hofmann, A. F., J. J. Middelburg, K. Soetaert, D. A. Wolf-Gladrow, and F. J. R. Meysman (2010), Proton cycling, buffering, and reaction stoichiometry in natural waters, *Mar. Chem.*, *121*, 246–255, doi:10.1016/j.marchem.2010.05.004.

Honjo, S., R. Francois, S. J. Manganini, J. Dymond, and R. Collier (2000), Particle fluxes to the interior of the Southern Ocean in the Western Pacific sector along 170°W, *Deep-Sea Res. II*, *47*, 3521–3548, doi:10.1016/S0967-0645(00)00077-1.

Hunt, B. P. V., E. A. Pakhomov, G. W. Hosie, V. Siegel, P. Ward, and K. Bernard (2008), Pteropods in Southern Ocean ecosystems, *Prog. Oceanogr.*, *78*, 193–221, doi:10.1016/j.pocean.2008.06.001.

Keir, R. S. (1980), The dissolution kinetics of biogenic calcium carbonates in seawater, *Geochim. Cosmochim. Acta*, *44*, 241–252, doi:10.1016/0016-7037(80)90135-0.

Laws, E. A., P. G. Falkowski, W. O. Smith, Jr., H. Ducklow, and J. J. McCarthy (2000), Temperature effects on export production in the open ocean, *Global Biogeochem. Cycles*, *14*, 1231–1246, doi:10.1029/1999GB001229.

Martin, J. H., G. A. Knauer, D. M. Karl, and W. W. Broenkow (1987), VERTEX: carbon cycling in the northeast Pacific, *Deep Sea Res. A*, *34*, 267–285, doi:10.1016/0198-0149(87)90086-0.

Martin, W. R., and F. L. Sayles (2003), 7.02 - The recycling of biogenic material at the seafloor, in Treatise on Geochemistry, edited by H. D. Holland and K. K. Turekian, pp. 37–65, Pergamon, Oxford, U. K., doi:10.1016/B0-08-043751-6/07089-4.

McNeil, B. I., and R. J. Matear (2008), Southern Ocean acidification: A tipping point at 450-ppm atmospheric CO_2, *Proc. Natl. Acad. Sci. U S A*, *105*, 18,860–18,864, doi:10.1029/2007GB002991.

McNeil, B. I., N. Metzl, R. M. Key, R. J. Matear, and A. Corbiere (2007), An empirical estimate of the Southern Ocean air-sea CO_2 flux, *Global Biogeochem. Cycles*, *21*, GB3011, doi:10.1029/2007GB002991.

Orr, J. C., et al. (2005), Anthropogenic ocean acidification over the twenty-first century and its impact on calcifying organisms, *Nature*, *437*, 681–686, doi:10.1038/nature04095.

Peng, T. H., W. S. Broecker, G. Kipphut, and N. Shackleton (1977), Benthic mixing in deep sea cores as determined by ^{14}C dating and its implications regarding climate stratigraphy and the fate of fossil fuel CO_2, in The Fate of Fossil Fuel CO_2 in the Oceans, edited by N. R. Anderson and A. Malahoff, pp. 355–373, Plenum, New York.

Pilskaln, C. H., S. J. Manganini, T. W. Trull, L. Armand, W. Howard, V. L. Asper, and R. Massom (2004), Geochemical particle fluxes in the Southern Indian Ocean seasonal ice zone: Prydz Bay region, East Antarctica, *Deep-Sea Res. I*, *51*, 307–332, doi:10.1016/j.dsr.2003.10.010.

Sachs, O., E. J. Sauter, M. Schlüter, M. M. Rutgers van der Loeff, K. Jerosch, and O. Holby (2009), Benthic organic carbon flux and oxygen penetration reflect different plankton provinces in the Southern Ocean, *Deep Sea Res. Part I*, *56*, 1319–1335, doi:10.1016/j.dsr.2009.02.003.

Steinacher, M., F. Joos, T. L. Fröhlicher, G. K. Plattner, and S. C. Doney (2009), Imminent ocean acidification in the Arctic projected with the NCAR global coupled carbon cycle-climate model, *Biogeosciences*, *6*, 515–533, doi:10.5194/bg-6-515-2009.

Stow, C. A., J. Jolliff, D. J. McGillicuddy, S. C. Doney, J. I. Allen, M. A. M. Friedrichs, K. A. Rose, and P. Wallhead (2009), Skill assessment for coupled biological/physical models of marine systems, *J. Mar. Syst.*, *76*, 4–15, doi:10.1016/j.jmarsys.2008.03.011.

Sundquist, E. T. (1985), Geological perspectives on carbon dioxide and the carbon cycle, in The Carbon Cycle and Atmospheric CO_2: Natural Variations Archean to Present, Geophys. Monogr. Ser, vol. 32, edited by E. T. Sundquist and W. S. Broecker, pp. 5–59, AGU, Washington, D. C.

Takahashi, T., et al. (2009), Climatological mean and decadal change in surface ocean pCO_2, and net sea-air CO_2 flux over the global oceans, *Deep-Sea Res. Part II Topical Stud. Oceanogr.*, *56*, 554–577, doi:10.1016/j.dsr2.2008.12.009.

Timmermann, R., et al. (2010), A consistent data set of Antarctic ice sheet topography, cavity geometry, and global bathymetry, *Earth Syst. Sci. Data*, *2*, 261–273, doi:10.5194/essd-2-261-2010.

Valsala, V., and S. Maksyutov (2010), Simulation and assimilation of global ocean pCO_2 and air-sea CO_2 fluxes using ship observations of surface ocean pCO_2 in a simplified biogeochemical offline model, *Tellus Ser. B Chem. Phys. Meteorol.*, *62*, 821–840, doi:10.1111/j.1600-0889.2010.00495.x.

Wefer, G., and G. Fischer (1991), Annual primary production and export flux in the Southern Ocean from sediment trap data, *Mar. Chem.*, *35*, 597–613, doi:10.1016/S0304-4203(09)90045-7.

Wefer, G., G. Fischer, D. Fütterer, and R. Gersonde (1988), Seasonal particle flux in the Bransfield Strait, Antarctica, *Deep-Sea Res.*, *35*, 891–898.

Wefer, G., G. Fischer, D. K. Fütterer, R. Gersonde, S. Honjo, and D. Ostermann (1989), Particle sedimentation and productivity in Antarctic waters of the Atlantic sector, in Geological History of the Polar Oceans—Arctic versus Antarctic, edited by U. Bleil and J. Thiede, pp. 363–379, Kluwer Academic Publ., Dordrecht.

Yamamoto-Kawai, M., F. A. McLaughlin, E. C. Carmack, S. Nishino, and K. Shimada (2009), Aragonite undersaturation in the Arctic Ocean: Effects of ocean acidification and sea ice melt, *Science*, *326*, 1098–1100, doi:10.1126/science.1174190.

Yamanaka, Y., and E. Tajika (1996), The role of the vertical fluxes of particulate organic matter and calcite in the oceanic carbon cycle: Studies using an ocean biogeochemical general circulation model, *Global Biogeochem. Cycles*, *10*, 361–382, doi:10.1029/96GB00634.

Zeebe, R. E., and D. A. Wolf-Gladrow (2001), CO_2 in seawater: Equilibrium, kinetics, isotopes, no. 65 in Elsevier Oceanography Series, 346 pp., Elsevier, New York.